Applications of Artificial Neural Network (ANN) method for performance prediction of the effect of a vertical 90º bend on an air–silicone oil flow

P.O. Ayegba[1], M. Abdulkadir*[1], V. Hernandez-Perez[3], I. S. Lowndes[2], and B. J. Azzopardi[2]
[1] Department of Chemical Engineering, Federal University of Technology, Minna, Nigeria
[2]Fluid and Thermal Engineering Research Group, Faculty of Engineering, University of Nottingham United Kingdom
[3]Department of Mechanical Engineering, National University of Singapore
*Email of the corresponding author: paulsnow4christ@gmail.com

Abstract: Knowledge of how the presence of a bend can change the flow patterns of a gas–liquid mixture is important for the design of multiphase flow systems, particularly to prevent burn-out and erosion–corrosion. Burn-out and erosion–corrosion both have serious implications for heat and mass transfer. The objective of this work therefore is to train an artificial neural network (ANN), a powerful interpolation technique, to predict the effect of a vertical 90º bend on an air–silicone oil mixture over a wide range of flow rates. Experimental data for training, validation, testing and final prediction were obtained using advanced instrumentation, wire mesh sensor (WMS) and high speed camera. The performance of the models were evaluated using the mean square error (*MSE*), average absolute relative error (*MAE*), Chi square test (X^2) and cross correlation coefficients (R). The performance discriminator X^2 for prediction of average void fraction is 2.57e-5 and that for probability density function (PDF) of void fraction *MAE* is 0.0028 for best performing models. The well trained ANN is then used to predict the effects of the two input parameters individually. The predicted results show that for the before the bend scenario, the most effective input parameter that reflects a change in flow pattern is the gas superficial velocity. On the other hand, the most unfavourable output parameter to measure after the bend is the average void fraction based on the fact that the flow near the bend is a developing one.
Key words: 90º bend; air–silicone oil; void fraction; PDF; ANN; modelling

I. Introduction

Pipe fittings such as valves, bends, elbows, tees, reducers, expanders, are integral parts of any piping system. Flow through piping components is more complex than in straight pipes [1]. The presence of a bend can significantly change the flow patterns immediately downstream with the potential of causing damage to the pipe. One common multiphase flow characteristic observed in flows is the redistribution of the flow phases within the bend. This may lead to secondary flows, strongly fluctuating void fractions, flow excursions, flow separations, pressure pulsations and other unsteady flow phenomena [2]. The requirements for economic design, optimization of operating conditions, and evaluation of safety factors create the need for quantitative information about such flows [2].

The possibility of using experimental data to train an Artificial Neural Network (ANN) in order to predict the redistribution of multiphase flows passing through 90º bends, has received little attention in the peer review literature. Most of the investigations have been restricted to experimental investigation: [2–8] address the issue of gas–liquid systems but most of the reported experiments are not extended to the application of ANN to predict such flows in bends. This paper extends experimental investigation [2] to consider the application of ANN to predict the redistribution of multiphase flows in 90º bends.

Transport processes such as mass, momentum and heat transfer during two-phase gas–liquid flow are vastly influenced by the flow characteristics. For an overall performance and purpose of safety in industrial systems, such as petroleum,

biomedical processing systems, chemical and nuclear reactors, it is essential to monitor the flow behaviour during normal and transient operations [9]. According to [9], accurate knowledge of flow pattern is necessary in design analysis and rig operation. Probability density function (PDF) of void fraction has been successfully used in the past to characterise flow patterns [8–14]. A number of studies have been carried out on the application of ANN for predicting flow characteristics. [15–21] applied ANN for the prediction of hydrodynamic parameters in gas-liquid flow. These studies were limited to flow through straight pipes, however [22] applied ANN for the prediction of frictional pressure drops in U-bends. They claimed that the ANN accurately predicted frictional pressure drop across U-bends.

In general, ANN is widely used in function estimation since it is able to estimate virtually any function in a stable and efficient manner [17]. Therefore, it is expected that the ANN approach can predict the major performance of the effect of bends at arbitrary input conditions without experiment measurements in more industry relevant fluids for the optimal, efficient and safe operation of the flow systems.

II. Material and Methods

All experiments were carried out on an inclinable pipe flow rig available within the Engineering Laboratories of the University of Nottingham. Details about the experimental apparatus have been previously reported by [2,23–25]. The experiments were all performed at an ambient laboratory temperature of 20 ± 0.5 ^{o}C and a pressure of 1 bar. The behaviour of the air– silicone oil mixture was examined using WMS. This technology, described by [26–28], can image the dielectric components in the pipe flow phases by measuring rapidly and continually the capacitances of the passing flow across several crossing points in the mesh.

1. Artificial neural network (ANN) modelling

In this work, three different training algorithms from commercial application (MATLAB) were used to configure the network and three different transfer functions (tansig, logsig and purelin) were tested for each training algorithm. The network topography consists of an input layer *IL*, a hidden layer *HL* and an output layer *OL*. The three training algorithms used are; Gradient descent with variable step size and momentum term (GDX); Levenberg Marquardt (LM) algorithm and Resilient back-propagation (RP). Through reliable training and testing using experimental data, the trained ANN can predict the performance of the effect of a bend on air–silicone oil flow. When the ANN is applied to predict the performance of the effect of a bend, it can reveal the highly non-linear relationship between the two input

parameters and two output parameters, by searching for optimum weights in its weighting space. Searching for optimal weights or training the ANN aims to minimize a cost function with respect to the training data set. The mathematical background can be found in [12,21,22]. It is worth mentioning that different network topologies are available in ANN but for this work, the back-propagation network with feed-forward algorithm was chosen as this has performed satisfactorily well in previous works [16,18,20,29,30].

III. Results and Discussion

1. Variation of MSE with number of processing elements in the *HL*

Table 1 presents the optimum number of processing elements for average void fraction and PDF of void fraction before and after the bend. The number of processing elements which gives the least value of minimum cross-validation *MSE* is chosen as optimum.

Objective function and performance of ANN

The objective function provides the basis for performance evaluation and network algorithm selection. In this work, sum of squares of error is used as the objective function and is given by equation (1).

TABLE 1: OPTIMUM NUMBER OF NEURONS

Algorithm	Transfer function	Optimum number of processing elements			
		Average void fraction (ε)		PDF of void fraction	
		Before the bend	After the bend	Before the bend	After the bend
GDX	Tansig	4	8	12	11
	Logsig	9	10	12	11
	Purelin	16	2	18	13
LM	Tansig	17	20	12	11
	Logsig	8	6	12	27
	Purelin	6	2	18	16
RP	Tansig	10	14	12	5
	Logsig	8	3	12	14
	Purelin	3	2	11	16

$$E = \frac{1}{2}\sum_{i=1}^{N}(O_i - t_i)^2 \quad (1)$$

Equations (2–5) are used to check the overall performance of the network. Mean Square Error (*MSE*), given by;

$$MSE = \frac{1}{N}\sum_{i=1}^{N}(O_i - t_i)^2 \quad (2)$$

Mean Absolute Error (*MAE*), given by;

$$MAE = \frac{1}{N}\sum_{i=1}^{N}|O_i - t_i| \quad (3)$$

Chi square test

$$X^2 = \sum_{i=1}^{N}\frac{(O_i - t_i)^2}{t_i} \quad (4)$$

Correlation Coefficient

$$R = \frac{\sum_{i=1}^{N}(O_i - \bar{O})(t_i - \bar{t})}{\sqrt{\sum_{i=1}^{N}(O_i - \bar{O})^2 \sum_{i=1}^{N}(t_i - \bar{t})^2}} \quad (5)$$

The maximum validation test is chosen as six (6) as this produced good results for the problems tested. Network configuration was based on minimum cross validation *MSE*. It is worth mentioning that the model with the least value of Chi square (X^2) is taken as the model with best performance when predicting average void fraction. On the other hand, the prediction of PDF of void fraction model performance is based on the Mean Absolute Error (*MAE*). Thus, the model with the least value of *MAE* is chosen as the model with the best performance.

2. Performance for test and prediction data sets

In this work, test and prediction data sets are used for testing model performance. However, it is worthy of note that while test data set was part of the original network configuration, the prediction data set was not. Since the prediction data set is not included during network configuration, results obtained from it can be used reliably to validate model results obtained from test data, thus minimising the risk of randomization error. While the test data is used here to choose the best performing model, the prediction data set serves as a check for generalization properties of the model.

It can be observed from Table 2 (test data) that all the ANN models tested for the prediction of average void fraction before the bend performed very well. This is seen in the small values of *MAE* and closeness to unity of *R*. However, Chi square test confirms that the ANN model based on LM algorithm with logsig transfer function and 8 neurons in the hidden layer performed best for the prediction of average void fraction before the bend. Results of Table 2 (prediction data) are a confirmation that all the models tested performed satisfactorily and that the models have good generalization properties.

TABLE 2: PERFORMANCE OF ANN MODELS FOR PREDICTION OF AVERAGE VOID FRACTION BEFORE THE BEND

	Algorithm	Transfer function	Measurement Type (Test data)				Measurement Type (Prediction data)			
			MSE	*MAE*	*R*	Chi square	*MSE*	*MAE*	*R*	Chi square
Average void fraction	GDX	Tansig	0.0014	0.1915	0.9864	0.0089	0.0015	0.0527	0.9907	0.0021
		Logsig	0.0034	0.2616	0.9902	0.0181	0.0016	0.0521	0.9714	0.0025
		Purelin	0.0107	0.5894	0.9189	0.1113	0.0078	0.1237	0.9542	0.0125
	LM	Tansig	2.50e-4	0.0414	0.9991	5.36e-4	0.0100	0.1119	0.8060	0.0136
		Logsig	9.82e-6	0.0057	0.9999	2.57e-5	5.56e-4	0.0313	0.9674	8.13e-4
		Purelin	0.0110	0.5970	0.9189	0.1156	0.0076	0.1216	0.9541	0.0122
	RP	Tansig	0.0061	0.4141	0.9479	0.0457	4.50e-4	0.0277	0.9694	6.31e-4
		Logsig	0.0014	0.1602	0.9949	0.0067	0.0025	0.0610	0.9410	0.0038
		Purelin	0.0114	0.6143	0.9148	0.1113	0.0130	0.1675	0.9465	0.0204

Table 3 gives performance results for best ANN models for prediction of PDF of void fraction before the bend. It is observed that the ANN model based on LM algorithm with sigmoid transfer function in the *HL* performed very well as can be seen by the small values of *MAE* and the closeness of *R* to unity. This is further validated by similar results obtained for prediction data.

TABLE 3: PERFORMANCE OF BEST ANN MODELS FOR PREDICTION OF PDF OF VOID FRACTION BEFORE THE BEND

Algorithm	Transfer function	Measurement Type (Test data)			Measurement Type (Prediction data)		
		MSE	*MAE*	*R*	*MSE*	*MAE*	*R*
GDX	Tansig	3.5041e-4	0.0106	0.5287	2.3702e-4	0.0113	0.5556
	Logsig	2.7497e-4	0.0094	0.6202	1.4472	0.0091	0.5718
	Purelin	3.3954e-4	0.0098	0.4922	1.6428	0.0096	0.4187
LM	Tansig	5.8107e-5	0.0028	0.9335	8.4041e-6	0.0019	0.9750
	Logsig	7.0600e-5	0.0029	0.9189	1.5103e-5	0.0026	0.9550
	Purelin	3.1843E-4	0.0077	0.5413	1.0143e-4	0.0067	0.6441
RP	Tansig	2.0835e-4	0.0065	00.730	1.9297e-4	0.0063	0.6372
	Logsig	2.6266e-4	0.0072	0.6506	1.0159e-4	0.0052	0.7614
	Purelin	2.9992e-4	0.0074	0.5768	1.1360e-4	0.0075	0.5987

Comparison between experimental and predicted PDF of void fraction before the bend

According to [14], a single peak at low void fraction represents bubbly flow whiles a single peak at low void fraction accompanied by a broadening tail represents spherical cap bubble. On the other hand a double peak feature with one

at low void fraction and the other at high void fraction represents slug flow. However, a single peak at high void fraction with a broadening tail represents churn flow.

Figure 1 shows the comparison between experimental and predicted PDF of void fraction before the bend at liquid and gas superficial velocities of 0.14 $m\,s^{-1}$ and (0.05 – 2.84) $m\,s^{-1}$, respectively.

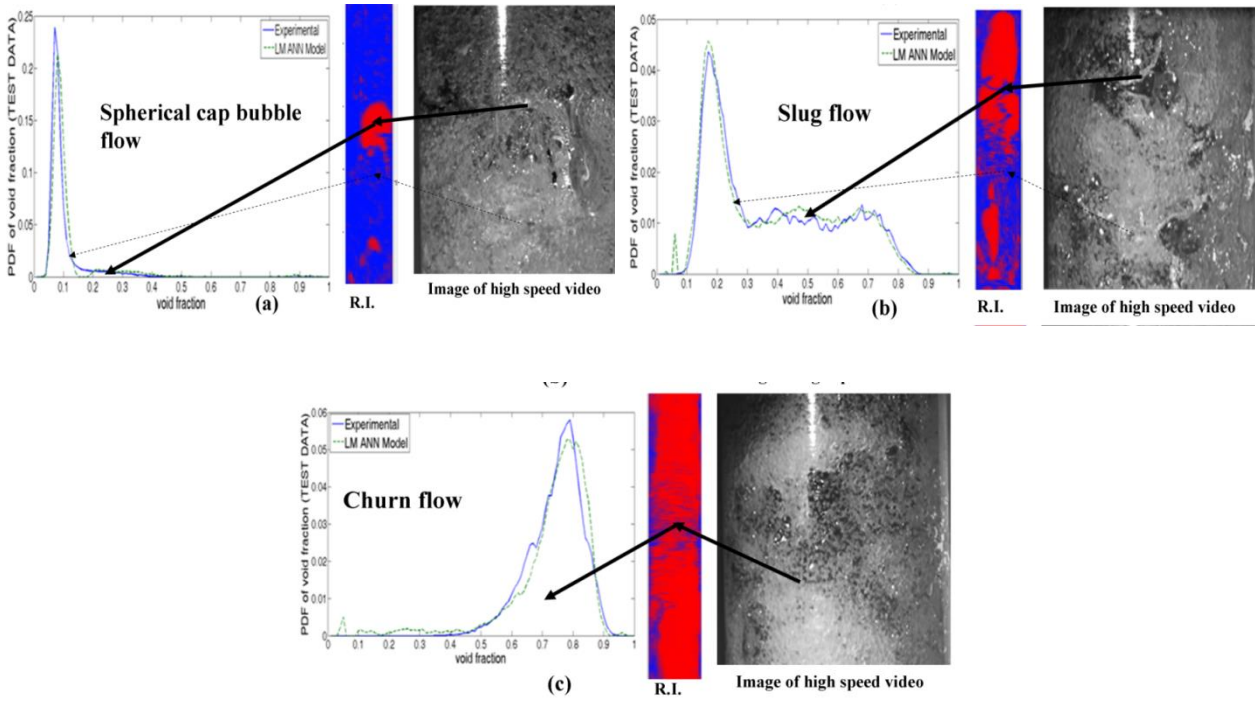

Figure 1: Experimental and predicted PDF of void fraction before the bend at liquid superficial velocity of 0.14 and gas superficial velocity ($m\,s^{-1}$) of: (a) 0.05 (b) 0.54 and (c) 2.84. R.I. represents reconstructed images of two-phase flow pattern. The dash line (a) Represents bubble flow whiles the thick line spherical cap bubble. On the other hand, the thick line in (b) represents Taylor bubble whiles the dash line liquid slug. The thick line in (c) represents churn flow.

From the plot, at liquid and gas superficial velocities of 0.14 $m\,s^{-1}$ and 0.05 $m\,s^{-1}$, respectively, both the experimental and predicted PDF of void fraction presents a single peak at low void fraction with a broadening tail extending to a high value of 0.4. This defines a spherical cap bubble flow as in [14]. The flow pattern has been confirmed by the reconstructed images of gas–liquid flow patterns and images of high speed video as shown in Figure 1 a. Thus the degree of agreement between experimental and predicted ANN is good.

When the gas superficial velocity increases to 0.54 $m\,s^{-1}$, the spherical cap bubbles coalesce into bullet-shaped Taylor bubbles and a slug regime is formed. Both the experiment and ANN model (predicted) gives two main peaks at the

values of 0.20 and 0.70, respectively. These peaks are the signature of the aerated liquid slugs and the Taylor bubbles with the different sizes. This is also confirmed by the analysis of the reconstructed images of two-phase flow pattern and video images as depicted in Figure 1 b.

At 2.84 $m\ s^{-1}$ gas superficial velocity, both the experimental and predicted PDF of void fraction shows a single peak at void fraction of about 0.80 with broadened tails, down to 0.3 and 0.92. This is the typical feature of churn.

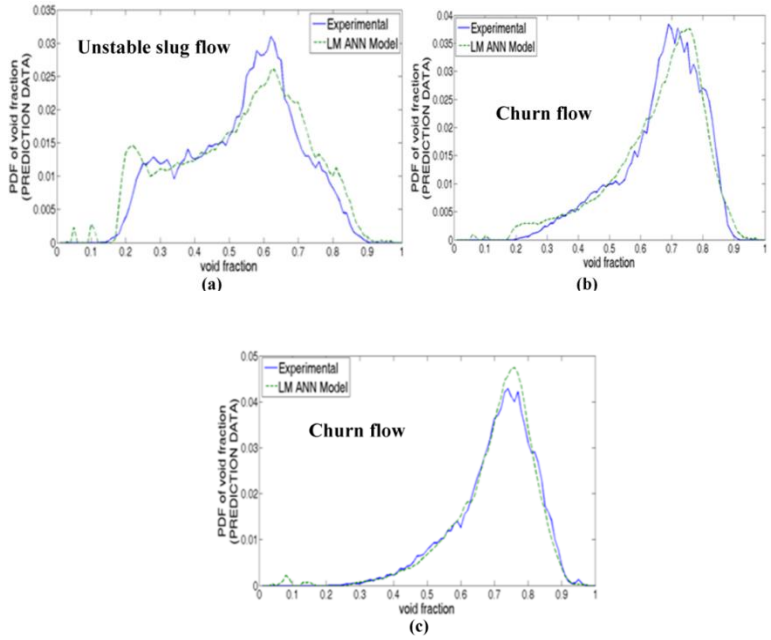

Figure 2: Experimental and predicted PDF of void fraction at liquid superficial velocity of 0.14 and gas superficial velocity ($m\ s^{-1}$) of: (a) 0.95 (b) 1.40 and (c) 1.89.

It is worth mentioning that during the course of carrying out the experimental campaign, it was observed that, the structure of churn flow becomes unstable with the fluid travelling up and down in an oscillatory fashion but with a net upward flow. The instability can be attributed to the relative parity between gravity and shear force acting in opposing direction to the thin film of liquid of Taylor bubbles. Thus, the question begging for an answer therefore here is can the ANN model successfully mimic churn flow and the transition from slug to churn flow (unstable slug flow) with confidence? This section, aims to provide an answer to this interesting question which has serious implications for heat and mass transfer using the PDF of void fraction presented in Figure 2.

Interestingly, the ANN model is able to replicate both the unstable slug and churn flows as shown in Figure 2. At gas superficial velocity of 0.95 $m\ s^{-1}$, two peaks appear on both the experimental and predicted PDF graph of void fractions. The high value of gas flow rate of 0.95 $m\ s^{-1}$ brings out an increase in Taylor bubbles and the shrinkage of

the liquid slugs and as a consequence more and more bubbles are entrained in the liquid slugs. This pattern according to [14] is defined as unstable slug flow.

When the gas superficial velocity reaches 1.40 $m\ s^{-1}$, the PDF of void fraction for both the experimental and predicted have a single peak with broadened tails down to 0.2 and 0.9. This is the typical feature of churn flow.

At gas superficial velocity of 1.89 $m\ s^{-1}$, the flow pattern for both the experiment and predicted remain unchanged, churn flow.

Table 4 presents a summary of comparison between experimental and predicted PDF of void fraction before the bend. It can be concluded therefore that the model can be used to predict unstable slug and churn flows before the bend with confidence.

TABLE 4: SUMMARY OF COMPARISON BETWEEN EXPERIMENTAL AND PREDICTED PDF OF VOID FRACTION BEFORE THE BEND FOR BOTH TEST AND PREDICTION DATA SETS

Flow condition	Test data		Flow condition	Prediction data	
	Experimental	Predicted		Experimental	Predicted
U_{SL}= 0.05 $m\ s^{-1}$ U_{SG}= 0.34 $m\ s^{-1}$	Slug flow	Slug flow	U_{SL}= 0.05 $m\ s^{-1}$ U_{SG}=1.42 $m\ s^{-1}$	Churn flow	Churn flow
U_{SL}= 0.14 $m\ s^{-1}$ U_{SG}= 0.05 $m\ s^{-1}$	Spherical cap bubble	Spherical cap bubble	U_{SL}= 0.05 $m\ s^{-1}$ U_{SG}=1.89 $m\ s^{-1}$	Churn flow	Churn flow
U_{SL}= 0.14 $m\ s^{-1}$ U_{SG}=0.54 $m\ s^{-1}$	Slug flow	Slug flow	U_{SL}= 0.05 $m\ s^{-1}$ U_{SG} =2.84 $m\ s^{-1}$	Churn flow	Churn flow
U_{SL}= 0.14 $m\ s^{-1}$ U_{SG} =2.84 $m\ s^{-1}$	Churn flow	Churn flow	U_{SL}= 0.14 $m\ s^{-1}$ U_{SG}= 0.95 $m\ s^{-1}$	Unstable slug flow	Developing slug flow

Results of Tables 5 and 6 indicate that all the ANN models tested performed poorly and showed weak generalisation properties. This can be attributed to the fact that the flow immediately downstream of the bend is not fully developed. It is interesting, though, to observe from Table 6 that the ANN model based on gradient descent algorithm with *logsig* transfer function and eleven neurons in the *HL* performed better than all the other ANN models tested. It surmises to say that the ANN models cannot be used reliably in the prediction of average void fraction and PDF of void fraction immediately after the bend where the flow is not fully developed.

Tables 5 give performance results of the models tested for the prediction of average void fraction after the bend.

TABLE 5: PERFORMANCE OF BEST ANN MODELS FOR PREDICTION OF AVERAGE VOID FRACTION AFTER THE BEND

Algorithm	Transfer function	Measurement Type (Test data)	Measurement Type (Prediction data)

		MSE	*MAE*	*R*	*Chi square*	*MSE*	*MAE*	*R*	*Chi square*
GDX	Tansig	0.0485	0.9778	0.9886	0.2171	0.0106	0.1199	0.9995	0.0123
	Logsig	0.0438	0.9611	0.9993	0.2140	0.0047	0.0659	0.7381	0.0060
	Purelin	0.1055	1.5623	0.8477	0.6016	0.0084	0.0970	0.7477	0.0096
LM	Tansig	0.0346	0.9091	0.9402	0.2647	0.0205	0.1520	0.3408	0.0255
	Logsig	0.1151	1.4591	0.5549	0.5957	0.0147	0.1196	0.3619	0.0166
	Purelin	0.0893	1.3884	0.9047	0.4743	0.0064	0.0736	0.6506	0.0073
RP	Tansig	0.0164	0.2137	0.9972	0.0211	0.0113	0.1001	0.6951	0.0130
	Logsig	0.0841	1.4519	0.9911	0.4972	0.0036	0.0647	0.9901	0.0041
	Purelin	0.1013	1.5486	0.8797	0.5890	0.0042	0.0550	0.6941	0.0047

TABLE 6: PERFORMANCE OF BEST ANN MODELS FOR PREDICTION OF PDF OF VOID FRACTION AFTER THE BEND

Algorithm	Transfer function	Measurement Type			Measurement Type (Prediction data)		
		MSE	*MAE*	*R*	*MSE*	*MAE*	*R*
GDX	Tansig	0.0034	0.0195	0.4048	9.3338e-4	0.0155	0.2448
	Logsig	0.0030	0.0186	0.6248	9.5071e-4	0.0149	0.2379
	Purelin	0.0039	0.0209	0.1724	5.2901e-4	0.0167	0.1876
LM	Tansig	0.0048	0.0190	-0.3178	0.0015	0.0109	0.3937
	Logsig	0.0040	0.0211	0.1105	0.0017	0.0145	0.3728
	Purelin	0.0036	0.0189	0.3791	3.6641e-4	0.0099	0.5667
RP	Tansig	0.0039	0.0213	0.1984	2.0884e-4	0.0080	0.7803
	Logsig	0.0038	0.0217	0.2287	7.3632e-4	0.0157	0.2845
	Purelin	0.0037	0.0194	0.3156	3.3291e-4	0.0104	0.5769

Comparison of experimental and ANN predicted average void fraction over the entire experimental range of gas superficial velocities

An interesting observation made here is that ANN models are able to successfully predict the variation in average void fraction with gas superficial velocity. It can be concluded based on the plots that the best degree of agreement between experiment and predicted average void fraction is observed at liquid superficial velocity of 0.14 $m\ s^{-1}$, followed by at 0.38 $m\ s^{-1}$.

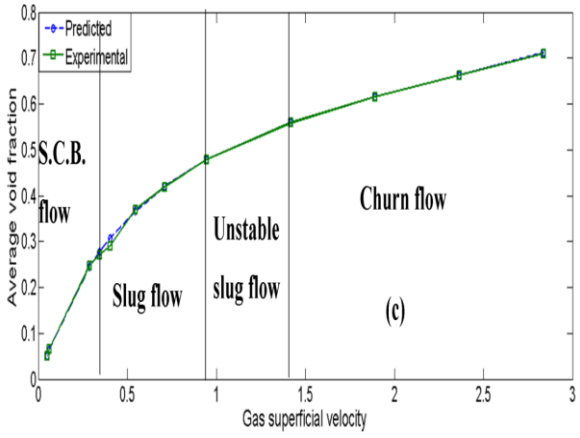

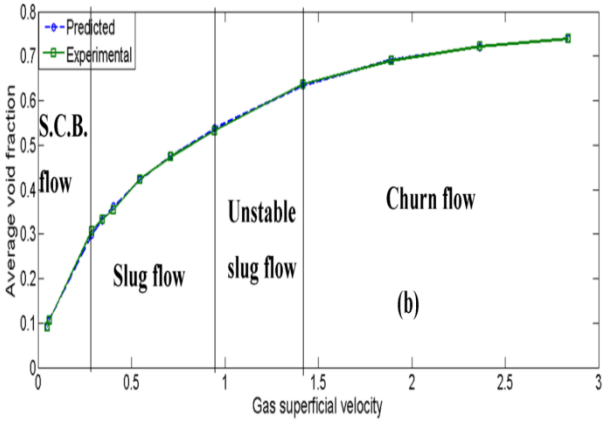

Figure 3: Comparison of variation of average void fraction with gas superficial velocity obtained from experiments and that predicted using the ANN model based on LM algorithm at liquid superficial velocity ($m\ s^{-1}$): (a) 0.14 and (b) 0.38.

Figure 3 (a and b) shows that both the experimental and predicted average void fraction changes with the gas superficial velocity whilst on the other hand decreases with liquid superficial velocity. From the plots, low void fraction values can be observed to be associated with spherical cap bubble and are seen to increase rapidly to slug, unstable slug and churn flows with an increase in gas superficial velocity. This observed trend with regards to average void fraction is consistent with the observations of [31–33].

IV. Conclusion

In this work, the applicability of the use of ANN for estimating the performance of the effect of a vertical 90^o bend on an air–silicone oil mixture was demonstrated. A well trained and tested ANN using measurement data is employed to predict its performance at off-design conditions. Especially, the effect of two input parameters (liquid and gas superficial velocities) has been examined. The performance discriminator X^2 for prediction of average void fraction is 2.57e-5 and that for PDF of void fraction *MAE* is 0.0028 for best performing models. This indicates that there is a good agreement between experimental and ANN predicted results. The predicted results show that the most effective positive influence on the bend is the gas superficial velocity. An increase in gas superficial velocity triggers a change in flow pattern from spherical cap bubble to slug flow then to churn flow and then finally to annular flow. Due to the capability of the neural networks to interpolate, it was applied successfully to predict void fraction outside the range of liquid and gas superficial velocities considered by the experimental work. Therefore, the void fraction and PDF of void fraction including the flow pattern can be predicted with a high degree of accuracy just by knowing the values of liquid and gas superficial velocities using ANNs.

References

1. Bandyopadhyay, T. K. & Das, S. K. Non-Newtonian pseudo-plastic liquid flow through small diameter piping comonents. *J. Pet. Sci. Eng.* **55,** 156–166 (2007).
2. Abdulkadir, M. *et al.* Interrogating the effect of 90o bends on air-silicone oil flows using advanced instrumentation. *Chem. Eng. Sci.* **66,** 2453–2467 (2011).
3. Gardner, G. C. & Neller, P. H. Phase distributions flow of an air-water mixture round bends and past obstructions. in *Proceedings of Institution of Mechanical Engineers* 93–101 (1969).
4. Carver, M. B. Numerical computation of phase separation in two fluid flow. *ASME Pap.* **6,** 153 (1984).
5. Carver, M. B. & Salcudean, M. Three-dimensional numerical modelling of phase distribution of two- fluid

flow in elbows and return bends. *Numer. Heat Transf.* **10,** 229–251 (1986).

6. Ellul, I. R. & Issa, R. I. Prediction of the flow of interspersed gas and liquid phases through pipe bends. *Trans. Inst. Chem. Eng.* **65,** 84–96 (1987).

7. Legius, H. J. W. M. & Van-den-Akker, H. E. A. Numerical and experimental analysis of translational gas-liquid pipe flow through a vertical bend. in *Proceedings of the 8th International Conference, BHR Group* (1997).

8. Saidj, F. *et al.* Experimental investigation of air-water two-phase flow through vertical 90 ° bend. *Exp. Therm. Fluid Sci.* **57,** 226–234 (2014).

9. Ghosh, S., Pratihar, D. K., Maiti, B. & Das, P. K. Identification of flow regimes using conductivity probe signals and neural networks for counter-current gas-liquid two-phase flow. *Chem. Eng. Sci.* **84,** 417–436 (2012).

10. Tutu, N. K. Pressure fluctuations and flow pattern recognition in vertical two-phase gas-liquid flows. International Journal of Multiphase flow. *Int. J. Multiph. Flow* **8,** 443 (1982).

11. Keska, J. K. & BE, W. Experimental comparison of flow pattern detection techniques for air-water mixture flow. *Exp. Therm. Fluid Sci.* **19,** 1–12 (1999).

12. Jones, O. C. & Zuber, N. The interrelation between void fraction fluctuations and flow pattern in two-phase flow. *Int. J. Multiph. flow* **2,** 273 (1975).

13. Vince, M. A. & Lahey, R. T. On the development of an objective flow regime indicator. International Journal of Multiphase Flow. *Int. J. Multiph. Flow* **8,** 93–124 (1982).

14. Costigan, G. & Whalley, P. B. Slug flow regime identification from dynamic void fraction measurements in vertical air-water flows. *Int. J. Multiph. Flow* **23,** 263–282 (1997).

15. Nasseh, S., Mohebbi, A., Jeirani, Z. & Sarrafi, A. Predicting pressure drop in venturi scrubbers with artificial neural networks. *J. Hazard. Mater.* **143,** 144–149 (2007).

16. Zhigiang, S. & Z. Hongjian. Neural networks approach for prediction of gas–liquid two-phase flow pattern based on frequency domain analysis of vortex flow meter signals. *Meas. Sci. Technol.* **19,** 1–8 (2008).

17. Kumar, A. & Kumar, G. K. Artificial neural network based prediction of bed expansion ratio in gas–solid fluidized beds with disk and blade promoters. *Journal* **85,** 12 – 16 (2004).

18. Ayoub, M. A. & Demiral, B. M. Application of Resilient Back-Propagation Neural Networks for Generating a Universal Pressure Drop Model in Pipelines. *Univ. KHARTOUM Eng. J.* **1,** 9–21 (2011).

19. Santoso, B. & Thomas, S. W. The Identification of Gas-liquid Co-current Two Phase Flow Pattern in a Horizontal Pipe Using the Power Spectral Density and the Artificial Neural Network (ANN). *Mod. Appl. Sci.* **6,** 56–67 (2012).

20. Bar, N. & Das, S. K. Gas-non-Newtonian Liquid Flow Through Horizontal Pipe – Gas Holdup and Pressure Drop Prediction using Multilayer Perceptron. *Am. J. Fluid Dyn.* **2,** 7–16 (2012).

21. Bar., N. & Das, S. K. Prediction of flow regime for air-water flow in circular micro channels using ANN. *J. Pet. Sci. Eng.* **10,** 813–821 (2013).

22. Bar, N., Das, S. K. & Biswas, M. N. Prediction of Frictional Pressure Drop Using Artificial Neural Network for Air-water Flow through U-bends. *Procedia Technol.* **10,** 813–821 (2013).

23. Abdulkadir, M., Hernandez-Perez, V, ., Lo, S., Lowndes, I. S. & Azzopardi, B. J. Comparison of experimental and computational fluid dynamics (CFD) studies of slug flow in a vertical 90o bend. *J.*

Comput. Multiph. Flows **5,** 265–281 (2013).

24. Abdulkadir, M., Hernandez-Perez, V., Lowndes, I. S. & Azzopardi, B. J. Comparison of experimental and computational fluid dynamics (CFD) studies of slug flow in a vertical riser. *Exp. Therm. Fluid Sci.* **68,** 468–483 (2015).

25. Abdulkadir, M., Hernandez-Perez, V., Lowndes, I. S., Azzopardi, B. J. & Brantson, E. T. Detailed analysis of phase distributions in a vertical riser using wire mesh sensor (WMS). *Exp. Therm. Fluid Sci.* **59,** 32–42 (2014).

26. Azzopardi, B. J. *et al.* Wire mesh sensor studies in a vertical pipe. in *Fifth International Conference on Multiphase Systems* (2008).

27. Manera, A, Ozar, B., Paranjape, S., Ishii, M. & Prasser, H. –M. Comparison between wire-mesh-sensors and conducting needle-probes for measurements of two-phase flow parameters. *Nucl. Eng. Des.* **239,** 1718–1724 (2008).

28. Thiele, S., Da-Silva, M. J., Hampel, U., Abdulkareem, L. & Azzopardi, B. J. High-resolution oil-gas two-phase flow measurement with a new capacitance wire-mesh tomography. in *5th International Symposium on Process Tomography* 25–26 (2008).

29. Hao, Y. & Wilamowski, B. M. in *Industrial Electronics Handbook: INTELLIGENT SYSTEMS* 1–16 (Auburn University, 2010).

30. Mark, H. B., Martin, T. H. & Howard, B. D. Neural Network Toolbox (Matlab User's Guide, R2012b). 20–30 (2012).

31. Omebere-Iyari, N. K. Azzopardi, B. J. A study of flow patterns for gas/liquid flow in small diameter tubes. *Chem. Eng. Res. Des.* **85,** 180–192 (2007).

32. Bhagwat, S. M. & Ghajar, A. J. Similarities and differences in the flow patterns and void fraction in vertical upward and downward two phase flow. *Exp. Therm. Fluid Sci.* **39,** 213–227 (2012).

33. Oshinowo, T. & Charles, M. E. Vertical two-phase flow- Part 1: Flow pattern correlations. *Can. J. Chem. Eng.* **52,** 25–35 (1974).